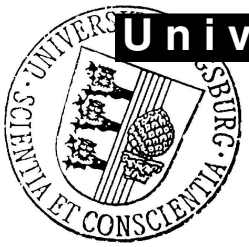

Universität Augsburg

Institut für
Mathematik

Ronald H.W. Hoppe, Svetozara I. Petrova

Shape Optimal Design of Periodic Microstructural Materials

Preprint Nr. 16/2008 — 07. April 2008
Institut für Mathematik, Universitätsstraße, D-86 135 Augsburg http://www.math.uni-augsburg.de/

Impressum:

Herausgeber:

Institut für Mathematik
Universität Augsburg
86135 Augsburg
http://www.math.uni-augsburg.de/forschung/preprint/

ViSdP:

Ronald H.W. Hoppe
Institut für Mathematik
Universität Augsburg
86135 Augsburg

Optimization Methods and Software
Vol. 00, No. 00, Month 200x, 1–18

Shape Optimal Design of Periodic Microstructural Materials

Ronald H.W. Hoppe[1,2] and Svetozara I. Petrova[1,3]
(Received 00 Month 200x; In final form 00 Month 200x)

[1] *Institute of Mathematics, University of Augsburg, Germany*

[2] *Department of Mathematics, University of Houston, TX 77204-3008, USA*

[3] *Institute for Parallel Processing, Block 25A, BAS, 1113 Sofia, Bulgaria*

We are concerned with shape optimal design of composite materials with periodic microstructures. The homogenization approach is applied to obtain the computationally feasible macromodel. The microstructural geometrical details of the microcells (such as lengths and widths of the different layers forming the cell walls) are considered as design parameters. They have a tremendous impact on the macroscopic behavior of the final produced composites. Our purpose is to find the best material-and-shape combination in order to achieve the optimal performance of the materials. The objective functional depends on the state variables describing the operational mode and the design parameters determining the shape. Our PDE constrained optimization routine is based on the elasticity problem as a state equation and additional equality and inequality constraints which are technically or physically motivated. The discretization of the PDE constrained optimization problem typically gives rise to a large-scale nonlinear programming problem. Primal-dual Newton-type interior-point methods are used for the numerical solution. The inequality constraints are treated by parameterized logarithmic barrier functions. The algorithm relies on an application of the adaptive path-following predictor-corrector method, inexact Newton solvers, and the all-at-once optimization approach. Numerical experiments are presented and discussed.

1 Introduction

This paper concerns an optimal shape design of periodic microstructural materials. In particular, we consider microcellular silicon carbide ceramics obtained by biotemplating which is a new technology used in the materials science to produce innovative devices and systems from biological materials. Our ceramic materials are derived from naturally grown wood by a two-step process involving pyrolysis of the wood, which results in a graphite-like carbonized preform, and a subsequent infiltration by liquid or gaseous silicon. The individual processing steps are shown in Figure 1.

Corresponding author. E-mail: petrova@math.uni-augsburg.de, Tel.: +49-821-5982312; Fax: +49-821-5982339.

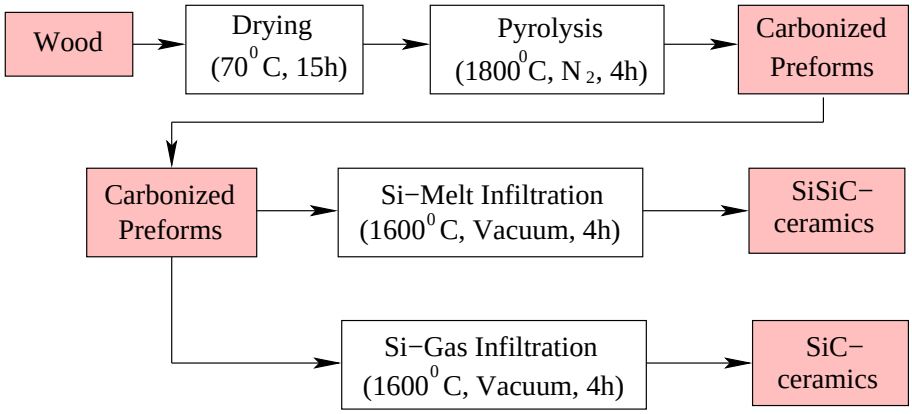

Figure 1. Processing scheme of SiSiC- and SiC-ceramics

The first step involves drying of the wood samples at 70^0C for about $15h$ followed by pyrolysis in N_2-atmosphere at 1800^0C taking approximately four hours. The weight loss of the wood preforms due to pyrolysis is in the range between 60% and 80% (e.g., ebony 64.6%, balsa 73.5%, and pine 73.8%). This goes along with an anisotropic shrinkage of about 40% in tangential, 30% in radial and 20% in axial direction which depends on the composition of the different cells in the tissue and the different orientation of the cellulose fibres in the cell walls. The total porosity of the resulting graphite-like carbonized preform is approximately 25% less than the initial porosity of the dried wood and features a multimodal pore size distribution with pores of a diameter between $1\mu m$ to $200\mu m$. The second stage of biotemplating consists of an infiltration of the biocarbon preforms by liquid or gaseous silicon at 1600^0C. After infiltration, the carbon structure is partially or completely converted into SiSiC-material (liquid infiltration) or β-SiC ceramics (gas infiltration). Note that despite the shrinkage and the change in porosity, the porous microstructures retain after the processing, see, Figure 2 (left) in case of a pyrolyzed pine specimen and Figure 2 (right) for a silicon-gas infiltrated pine preform.

The mechanical behavior of the final ceramics is largely determined by the geometry of its microstructure which can be very precisely tuned during the biotemplating process. The ultimate goal is to determine these microstructural details in such a way that an optimal mechanical performance is achieved with respect to merit criteria depending on the specific application. From a mathematical point of view, this amounts to a shape optimization problem where the state variables are the displacements subject to the underlying elasticity equations, and the design variables are the geometrical quantities determining the microstructure. Since a resolution of the microstructure is numerically cost-prohibitive, we perform homogenization techniques, assuming periodically

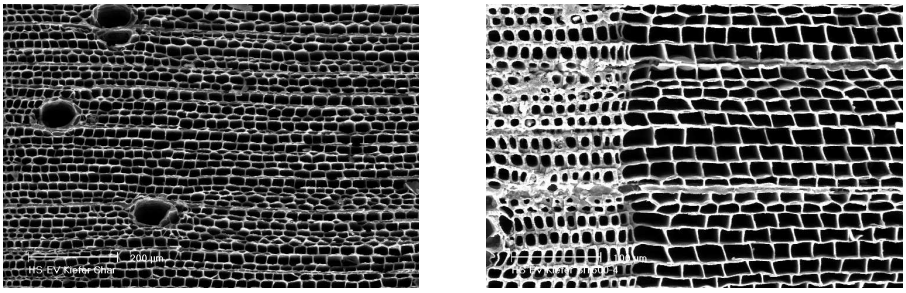

Figure 2. Microcellular biomorphic silicon carbide ceramics derived from natural wood: pyrolyzed pine template (left) and silicon-gas infiltrated pine (right)

distributed microcells, and apply state-of-the-art optimization methods to the homogenized model.

The paper is organized as follows: In Section 2 we elaborate on the homogenization technique that provides a macromechanical model where the components of the homogenized elasticity tensor reflect the microstructural details. In Section 3 we formulate the shape optimization problem subjected by equalities and inequalities constraints. Path-following interior-point method by means of an adaptive predictor-corrector type continuation algorithm is presented in Section 4 for the numerical solution of the optimization problem. Some numerical results are discussed in Section 5. Section 6 summarizes the results and gives concluding remarks.

2 Homogenization

Homogenization is a powerful mathematical tool to provide a model that appropriately describes the macroscopic behavior of periodically distributed microstructures. The standard approach relies on a two-scale asymptotic analysis (cf., e.g., [3, 5, 11, 15]).

As an idealization of the microstructure of the final silicon carbide ceramics, we assume the microcells to be periodically distributed and consider a specimen of macroscopic length L occupying a bounded domain Ω in Euclidean space $\mathbb{R}^2$. The periodicity cell Y is supposed to be of microscopic length $\ell \ll L$ consisting of a pore and different layers of materials, carbon (C) and silicon carbide (SiC), forming the cell walls (cf. Figure 3):

$$\begin{array}{lcll} Y & = & \text{Pore} \cup \text{SiC} \cup \text{C} & \text{(SiC/SiSiC-ceramics)} \\ Y & = & \text{Pore} \cup SiC & \text{(pure SiC-ceramics)} \end{array} .$$

Denoting by X the position vector, we introduce a macroscopic (slow) vari-

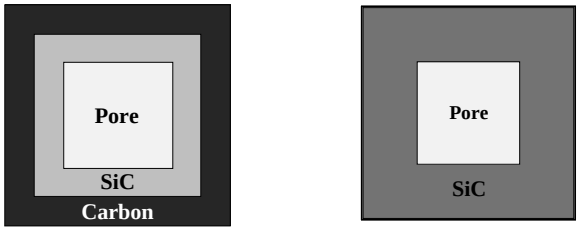

Figure 3. Periodicity cell Y: SiC-ceramics (left) and pure SiC-ceramics (right)

Table 1. Young's modulus and Poisson's ration

	Young's modulus (GPa)	Poisson's ratio
carbon	10	0.22
silicon carbide	410	0.14

able x and a microscopic (fast) variable y according to

$$\begin{array}{rcll} x & = & X/L & \text{(macroscopic (slow) variable)} \\ y & = & X/\ell & \text{(microscopic (fast) variable)} \end{array} \tag{1}$$

and refer to the ratio of the slow and the fast variable $\varepsilon := x/y = \ell/L \ll 1$ as the scale parameter. We assume linear elasticity in the periodicity cell Y

$$-\operatorname{div} \boldsymbol{\sigma}(X) \;=\; \mathbf{F}(X) \quad \text{in } Y \tag{2}$$

with periodic boundary conditions on ∂Y, where $\mathbf{F}$ stands for the load vector and the stress tensor $\boldsymbol{\sigma} = (\sigma_{ij})_{i,j=1}^{2}$ is related to the linearized strain tensor $\mathbf{e}(\mathbf{u}) = 0.5(\nabla\mathbf{u} + (\nabla\mathbf{u})^T)$ by Hooke's law

$$\boldsymbol{\sigma} \;=\; \boldsymbol{E}\ \mathbf{e}(\mathbf{u}). \tag{3}$$

Here, $\mathbf{u} = (u_1, u_2)^T$ denotes the displacements vector and $\boldsymbol{E} = (E_{ijk\ell})_{i,j,k,\ell=1}^{2}$ stands for the symmetric elasticity tensor which in case of plane stresses is given by

$$\begin{pmatrix} E_{1111} & E_{1122} & 0 \\ E_{2211} & E_{2222} & 0 \\ 0 & 0 & E_{1212} \end{pmatrix} \;=\; \frac{E}{1-\nu^2} \begin{pmatrix} 1 & \nu & 0 \\ \nu & 1 & 0 \\ 0 & 0 & 1-\nu \end{pmatrix} \quad , \tag{4}$$

where E and ν refer to Young's modulus and Poisson's ratio, respectively. Note that the coefficients $E_{ijk\ell}$ of the elasticity tensor $\boldsymbol{E}$ are discontinuous across material interfaces (see Table 1 which contains the values of E and ν

for the different materials).

We now consider the elasticity problem in the dimensionless macroscopic description, i.e., with regard to the macroscopic slow variable x. The displacement vector depends on the scale parameter ε and is denoted by $\mathbf{u}_\varepsilon$. Assuming prescribed normal stresses $\mathbf{t}$ on $\Gamma_T \subset \partial\Omega$ (see Figure 4) and prescribed displacements $\mathbf{g}$ on $\Gamma_D \subset \partial\Omega$, where $\partial\Omega = \Gamma_T \cup \Gamma_D$, $\Gamma_T \cap \Gamma_D = \emptyset$, the elasticity problem reads as follows:

$$-\text{ div } \boldsymbol{\sigma}_\varepsilon(x) = \mathbf{f}(x) \quad \text{in } \Omega, \tag{5}$$

$$\mathbf{n}(x) \cdot \boldsymbol{\sigma}_\varepsilon(x) = \mathbf{t}(x) \quad \text{on } \Gamma_T, \tag{6}$$

$$\mathbf{u}_\varepsilon(x) = \mathbf{g}(x) \quad \text{on } \Gamma_D, \tag{7}$$

where $\mathbf{n}$ refers to the unit outward normal and $\mathbf{u}_\varepsilon(x) := \mathbf{u}(x/\varepsilon)$, $\boldsymbol{\sigma}_\varepsilon(x) := \boldsymbol{E}_\varepsilon(x)\mathbf{e}(\mathbf{u}_\varepsilon(x))$, and $\boldsymbol{E}_\varepsilon(x) := \boldsymbol{E}(x/\varepsilon) = \boldsymbol{E}(y)$. For simplicity, in the sequel we assume $\mathbf{g} = 0$.

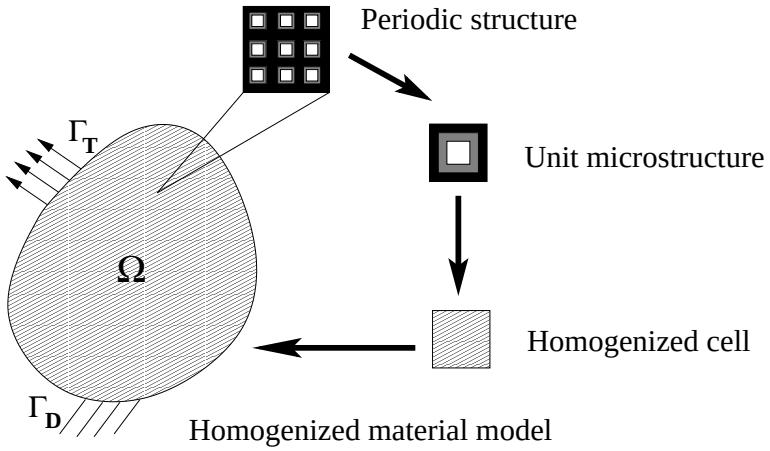

Figure 4. Domain occupied by microscopic homogenized material

We perform the double scale asymptotic expansion

$$\mathbf{u}_\varepsilon(x) \;=\; \mathbf{u}^{(0)}(x,y) \;+\; \varepsilon\mathbf{u}^{(1)}(x,y) \;+\; \varepsilon^2\mathbf{u}^{(2)}(x,y) \;+\; \ldots \quad , \tag{8}$$

where the vectors $\mathbf{u}^{(i)}(x,y)$, $i \geq 0$, are $Y-$periodic in y, i.e., take equal values on opposite sides of Y. Since $y = \varepsilon^{-1}x$, we can use the following differential

rules

$$\frac{d}{dx}G\left(x,\frac{x}{\varepsilon}\right)=\frac{\partial G(x,y)}{\partial x}+\varepsilon^{-1}\frac{\partial G(x,y)}{\partial y}.$$

In what follows, the subscripts x and y indicate the partial derivatives with respect to the space variables x and y, respectively. Then, the elasticity equation (5) reads

$$-\operatorname{div}_x\left(\boldsymbol{E}(y)\mathbf{e}_x(\mathbf{u}_\varepsilon)\right)=\mathbf{f}(x). \tag{9}$$

Replacing the solution $\mathbf{u}_\varepsilon$ from (8) in equation (9), one gets

$$-\left(\operatorname{div}_x+\varepsilon^{-1}\operatorname{div}_y\right)\Big\{\boldsymbol{E}(y)\Big((\mathbf{e}_x(\mathbf{u}^{(0)}+\varepsilon\,\mathbf{u}^{(1)}+\varepsilon^2\,\mathbf{u}^{(2)})+ \varepsilon^{-1}\mathbf{e}_y(\mathbf{u}^{(0)}+\varepsilon\,\mathbf{u}^{(1)}+\varepsilon^2\,\mathbf{u}^{(2)})\Big)\Big\}=\mathbf{f}(x),$$

which yields

$$-\left(\operatorname{div}_x+\varepsilon^{-1}\operatorname{div}_y\right)\Big\{\boldsymbol{E}(y)\Big(\varepsilon^{-1}\mathbf{e}_y(\mathbf{u}^{(0)})+\mathbf{e}_x(\mathbf{u}^{(0)})+\mathbf{e}_y(\mathbf{u}^{(1)})+ \varepsilon(\mathbf{e}_x(\mathbf{u}^{(1)})+\mathbf{e}_y(\mathbf{u}^{(2)}))+\varepsilon^2\mathbf{e}_x(\mathbf{u}^{(2)})\Big)\Big\}=\mathbf{f}(x).$$

Identify now the same powers of ε we arrive successively at the following problems

$$A_1\mathbf{u}^{(0)}=\mathbf{0}, \tag{10}$$

$$A_2\mathbf{u}^{(0)}+A_1\mathbf{u}^{(1)}=\mathbf{0}, \tag{11}$$

$$A_3\mathbf{u}^{(0)}+A_2\mathbf{u}^{(1)}+A_1\mathbf{u}^{(2)}=\mathbf{f}(x), \tag{12}$$

where the operators $A_i,\ i=1,2,3$, are defined as follows

$$\begin{aligned}A_1&:=-\operatorname{div}_y\left(\boldsymbol{E}(y)\,\mathbf{e}_y\right),\\ A_2&:=-\operatorname{div}_y\left(\boldsymbol{E}(y)\,\mathbf{e}_x\right)-\operatorname{div}_x\left(\boldsymbol{E}(y)\,\mathbf{e}_y\right),\\ A_3&:=-\operatorname{div}_x\left(\boldsymbol{E}(y)\,\mathbf{e}_x\right).\end{aligned}$$

The solution $\mathbf{u}^{(0)}(x,y)$ of (10) is Y-periodic in y and $A_1\mathbf{u}^{(0)}=\mathbf{0}$. Hence, $\mathbf{u}^{(0)}(x,y)$ is independent of y, i.e., $\mathbf{u}^{(0)}(x,y)=\mathbf{u}^{(0)}(x)$. Taking into account

that $\mathbf{e}_y(\mathbf{u}^{(0)}(x)) = \mathbf{0}$ the problem (11) results in

$$\mathrm{div}_y \left(\boldsymbol{E}(y)\mathbf{e}_x(\mathbf{u}^{(0)}) \right) + \mathrm{div}_y \left(\boldsymbol{E}(y)\mathbf{e}_y(\mathbf{u}^{(1)}) \right) = \mathbf{0}. \tag{13}$$

We look for $\mathbf{u}^{(1)}(x,y)$ as a linear vector function of $\mathbf{e}_x(\mathbf{u}^{(0)})$ in the form

$$\mathbf{u}^{(1)}(x,y) = -\boldsymbol{\xi}(y)\mathbf{e}_x(\mathbf{u}^{(0)}(x)) + \bar{\mathbf{u}}^{(1)}(x), \tag{14}$$

where $\bar{\mathbf{u}}^{(1)}(x)$ is an arbitrary function of x, $\boldsymbol{\xi}(y) = \boldsymbol{\xi}(y_1, y_2)$ is a third order tensor, $y-$depending and periodic in each argument, i.e., $\xi_p^{kl}(y_1, y_2)$ are supposed Y-periodic functions, $p, k, l = 1, 2$. From (13) and (14) one gets

$$\mathrm{div}_y \left(\boldsymbol{E}(y) - \boldsymbol{E}(y)\mathbf{e}_y(\boldsymbol{\xi}^{kl}) \right) = \mathbf{0}. \tag{15}$$

$\boldsymbol{\xi}(y)$ is defined up to an additive constant. For uniqueness we choose $\boldsymbol{\xi}(y)$ having zero mean value in Y, i.e., $< \boldsymbol{\xi}(y) >= 0$, where the volume average symbol is defined as

$$< * >:= |Y|^{-1} \int_Y * \, dY.$$

We solve then the equation (12) to find $\mathbf{u}^{(2)}$

$$A_1\mathbf{u}^{(2)} = \mathbf{f}(x) - A_3\mathbf{u}^{(0)} - A_2\mathbf{u}^{(1)}. \tag{16}$$

Compatibility condition for existence of a periodic solution $\mathbf{u}^{(2)}$ is given by the Fredholm equality

$$\int_Y \left(\mathbf{f}(x) - A_3\mathbf{u}^{(0)} - A_2\mathbf{u}^{(1)} \right) dy = \mathbf{0}, \qquad \forall x.$$

Successively we get

$$- \int_Y \mathrm{div}_x \left(\boldsymbol{E}(y)\mathbf{e}_x(\mathbf{u}^{(0)}) + \boldsymbol{E}(y)\mathbf{e}_y(\mathbf{u}^{(1)}) \right) dy = |Y|\, \mathbf{f}(x). \tag{17}$$

Replacing (14) in (17) and taking into account that $\mathbf{e}_y(\bar{\mathbf{u}}^{(1)}(x)) = \mathbf{0}$ the following expression holds

$$- \mathrm{div}_x \left(\left(\int_Y (\boldsymbol{E}(y) - \boldsymbol{E}(y)\mathbf{e}_y(\boldsymbol{\xi}^{kl})\, dy \right) \mathbf{e}_x(\mathbf{u}^{(0)}) \right) = |Y|\, \mathbf{f}(x). \tag{18}$$

Therefore, from (5) and (18), the homogenized elasticity tensor has the form

$$\boldsymbol{E}^H = \frac{1}{|Y|}\int_Y \Big(\boldsymbol{E}(y) - \boldsymbol{E}(y)\mathbf{e}_y(\boldsymbol{\xi}^{kl})\Big)\ dy\ =< \boldsymbol{E}(y) - \boldsymbol{E}(y)\mathbf{e}_y(\boldsymbol{\xi}^{kl}) >,$$

which by using summation on repeated index may be written in the sense of distributions as follows

$$E^H_{ijkl} = \frac{1}{|Y|}\int_Y \left(E_{ijkl}(y) - E_{ijpq}(y)\frac{\partial \xi^{kl}_p}{\partial y_q}\right)\ dy, \tag{19}$$

where $\xi^{k\ell}_p \in H^1_{per}(Y),\ k,\ell,p = 1,2$, is the Y-periodic solution of the cell problem

$$\int\limits_Y E_{ijpq}(y)\ \frac{\partial \xi^{k\ell}_p}{\partial y_q}\ \frac{\partial \Phi_i}{\partial y_j}\ dy = \int\limits_Y E_{ijk\ell}(y)\ \frac{\partial \Phi_i}{\partial y_j}\ dy\ ,\ \boldsymbol{\Phi} \in (H^1_{per}(Y))^2\ . \tag{20}$$

Theorem. Let $\mathbf{u}_\varepsilon \in \mathbf{H}^1_{0,\Gamma_D}(\Omega) := \{\mathbf{v} \in (H^1(\Omega))^2 \mid \mathbf{v}|_{\Gamma_D} = 0\}$ be the weak solution of the elasticity problem (5)-(7) with $\mathbf{g} = 0$, i.e.,

$$\int\limits_\Omega (E_\varepsilon)_{ijpq}(x)\ \frac{\partial (u_\varepsilon)_p}{\partial x_q}\ \frac{\partial (v_\varepsilon)_i}{\partial x_j}\ dx = \int\limits_\Omega \mathbf{f}\cdot\mathbf{v}_\varepsilon\ dx + \int\limits_{\Gamma_T}\mathbf{t}\cdot\mathbf{v}_\varepsilon\ ds\ ,\ \mathbf{v}_\varepsilon \in \mathbf{H}^1_{0,\Gamma_D}(\Omega),$$

where here and in the sequel we adopt Einstein's summation convention.

Then, the sequence $(\mathbf{u}_\varepsilon)_{\varepsilon>0}$ converges weakly to $\mathbf{u}^{(0)} \in (H^1(\Omega))^2$ as ε goes to 0, where the homogenized displacement vector $\mathbf{u}^{(0)}$ only depends on x and is the weak solution of the homogenized elasticity problem

$$-\ \mathrm{div}\ \boldsymbol{\sigma}(x) = \mathbf{f}(x) \quad \text{in } \Omega, \tag{21}$$

$$\mathbf{n}(x)\cdot\boldsymbol{\sigma}(x) = \mathbf{t}(x) \quad \text{on } \Gamma_T, \tag{22}$$

$$\mathbf{u}(x) = 0 \quad \text{on } \Gamma_D. \tag{23}$$

Here,

$$\boldsymbol{\sigma}(x)\ =\ \boldsymbol{E}^H\mathbf{e}_x(\mathbf{u}^{(0)}(x)) \quad ,\quad x \in \Omega, \tag{24}$$

where $\boldsymbol{E}^H = (E^H_{ijk\ell})^2_{i,j,k,\ell=1}$ stands for the homogenized elasticity tensor with coefficients $E^H_{ijk\ell}$ given by (19).

Proof: The assertions can be deduced following the lines of proof as in [3].

The computation of $\boldsymbol{\xi} = (\xi_p^{k\ell})_{k,\ell,p=1}^2$ as the solution of (20) cannot be done analytically for general configurations, but requires the use of numerical techniques.

3 Shape optimization

Shape optimization is by now a well established discipline in structural optimization (cf., e.g., [4, 7, 14, 16] and, in particular, [1] for shape optimization by homogenization). In this paper, the design objective involves an objective functional $J = J(\mathbf{u}, \boldsymbol{\alpha})$ depending on the state variables $\mathbf{u} = (u_1, \ldots, u_N)^T$, which are the nodal values of the components of the discrete displacement vector, and the design variables $\boldsymbol{\alpha} = (\alpha_1, \ldots, \alpha_M)^T$ chosen as the microstructural data determining the geometry of the periodicity cell (widths and lengths of the different layers forming the cell walls). Depending on the specific application, the objective functional can be chosen according to the various optimality criteria, for instance, loading (bending, tension, torsion), mechanical properties (minimum compliance), technological properties (minimum weight), thermal or economical specifications.

For a given objective functional J, the optimization problem can be stated as follows: Find $(\mathbf{u}, \boldsymbol{\alpha}) \in \mathbb{R}^N \times \mathbb{R}^M$ such that

$$J(\mathbf{u}, \boldsymbol{\alpha}) \;=\; \inf_{\mathbf{v}, \boldsymbol{\beta}} J(\mathbf{v}, \boldsymbol{\beta}) \tag{25}$$

subject to the equality constraints

$$A(\boldsymbol{\alpha})\, \mathbf{u} \;=\; \mathbf{f} \quad , \tag{26}$$

$$c(\boldsymbol{\alpha}) := \sum_{i=1}^{M} \alpha_i \;=\; C \;, \tag{27}$$

where (26) represents the discretized elasticity equations and (27) reflects a global constraint due to the geometry of the periodicity cell.

We further consider the inequality constraints

$$\alpha_{min}^{(i)} \;\leq\; \alpha_i \;\leq\; \alpha_{max}^{(i)} \quad , \quad 1 \leq i \leq M \quad , \tag{28}$$

which are given in terms of technologically motivated lower and upper bounds for the design parameters. We note that the stiffness matrix $A(\boldsymbol{\alpha}) = (a_{nm}(\boldsymbol{\alpha}))_{n,m=1}^N$ and the load vector $\mathbf{f} \in \mathbb{R}^N$ in (26) are given by

$$a_{nm}(\boldsymbol{\alpha}) = \sum_{K\in\mathcal{T}_h} \int\limits_K E^H_{ijk\ell}(\boldsymbol{\alpha})\ \frac{\partial \boldsymbol{\varphi}^m_k}{\partial x_\ell}\ \frac{\partial \boldsymbol{\varphi}^n_i}{\partial x_j}\ dx\ ,\ 1 \le n,m \le N\ , \tag{29}$$

$$b_n = \sum_{K\in\mathcal{T}_h} [\int\limits_K \mathbf{f}\cdot\boldsymbol{\varphi}^n\ dx + \int\limits_{\partial K\cap\Gamma_T} \mathbf{t}\cdot\boldsymbol{\varphi}^n\ ds]\ ,\ 1 \le n \le N\ , \tag{30}$$

where $(\boldsymbol{\varphi}^n)_{n=1}^N$ denotes the basis of the linear space $(S_{0,\Gamma_D}(\Omega;\mathcal{T}_h))^2$ of vector fields whose components are continuous, piecewise linear finite elements with respect to the simplicial triangulation $\mathcal{T}_h$ of the computational domain Ω vanishing on $\Gamma_D \cap \mathcal{T}_h$.

We further note that the dependence of the coefficients $E^H_{ijk\ell}(\boldsymbol{\alpha})$ of the homogenized elasticity tensor on the design variables cannot be computed analytically. In order to provide a sufficiently smooth dependence, which is needed within the solution of the shape optimization, we choose a uniform grid

$$\Pi_{\mathbf{k}} := \{\ \boldsymbol{\alpha} = (\boldsymbol{\alpha}^{(1)},\ldots,\boldsymbol{\alpha}^{(M)})\ |\ \alpha^{(i)}_j = \alpha^{(i)}_{min} + jk_i(\alpha^{(i)}_{max} - \alpha^{(i)}_{min})\ ,$$
$$0 \le j \le m_i\ ,\ k_i = (\alpha^{(i)}_{max} - \alpha^{(i)}_{min})/m_i\ ,\ 1 \le i \le M\ \}\ ,$$

of $\prod\limits_{i=1}^{M} [\alpha^{(i)}_{min}, \alpha^{(i)}_{max}] \subset \mathbb{R}^M$, compute the coefficients for $\boldsymbol{\alpha} \in \Pi_{\mathbf{k}}$ as the solution of the finite element discretized periodicity cell problems (20), and determine $E^H_{ijk\ell}(\boldsymbol{\alpha})$ as the multivariate spline interpolant with respect to the partition $\Pi_{\mathbf{k}}$.

The thus discretized shape optimization problem is solved by a one-shot method, also called all-at-once or all-in-one approach, where in contrast to more traditional optimization strategies the numerical solution of the discretized state equations (26) is an integral part of the optimization routine.

4 Path-following interior-point methods

Recently, primal-dual Newton-type interior-point methods have been used for the solution of nonlinear programming problems (cf., e.g., [6, 9, 10, 18]). We apply the path-following primal-dual approach based on adaptive continuation method by predictor-corrector steps.

The interior-point aspect is to couple the inequality constraints (28) by

logarithmic barrier functions

$$B^{(\mu)}(\mathbf{u},\boldsymbol{\alpha}) := J(\mathbf{u},\boldsymbol{\alpha}) - \frac{1}{\mu}\sum_{i=1}^{M}\left[\log(\alpha_i - \alpha_{min}^{(i)}) + \log(\alpha_{max}^{(i)} - \alpha_i)\right] , \quad (31)$$

where $\rho := 1/\mu > 0,\ \mu \to \infty$, is the barrier parameter. This leads to the following parameterized family of equality constrained minimization subproblems

$$\inf_{\mathbf{u},\boldsymbol{\alpha}} \ B^{(\mu)}(\mathbf{u},\boldsymbol{\alpha}) \quad (32)$$

subject to

$$A(\boldsymbol{\alpha})\,\mathbf{u} \ = \ \mathbf{f} \quad , \quad c(\boldsymbol{\alpha}) \ = \ C \ . \quad (33)$$

Assume that the sufficient smoothness of the objective functional, regularity of the equality and active inequality constraints, strict complementarity, and first and second order Karush-Kuhn-Tucker (KKT)-conditions are satisfied. It was proven (cf., e.g., [18]) that for sufficiently large $\mu > 0$ the subproblems (32)-(33) admit unique solutions $(\mathbf{u}^{(\mu)}, \boldsymbol{\alpha}^{(\mu)})$ which converge to a strict local minimum $(\mathbf{u}, \boldsymbol{\alpha})$ of (25)-(28) as $\mu \to \infty$.

The primal-dual aspect is to couple the equality constraints (33) by Lagrangian multipliers $\boldsymbol{\lambda}$ for the discretized state equations and η for the geometrical constraint resulting in the saddle point problem

$$\inf_{\mathbf{u},\boldsymbol{\alpha}} \ \sup_{\boldsymbol{\lambda},\eta} \ L^{(\mu)}(\mathbf{u},\boldsymbol{\alpha},\boldsymbol{\lambda},\eta) \ , \quad (34)$$

where the Lagrangian is given by

$$L^{(\mu)}(\mathbf{u},\boldsymbol{\alpha},\boldsymbol{\lambda},\eta) := B^{(\mu)}(\mathbf{u},\boldsymbol{\alpha}) + \boldsymbol{\lambda}^T(A(\boldsymbol{\alpha})\mathbf{u} - \mathbf{f}) + \eta\,(c(\boldsymbol{\alpha}) - C) \ . \quad (35)$$

The Karush-Kuhn-Tucker conditions with respect to (34) read as follows

$$\mathbf{F}^{(\mu)}(\boldsymbol{\psi}) := \mathbf{F}(\boldsymbol{\psi}(\mu),\mu) = \nabla L^{(\mu)} = \mathbf{0}, \quad (36)$$

where $\nabla L^{(\mu)} = \left(L_{\mathbf{u}}^{(\mu)}, L_{\boldsymbol{\alpha}}^{(\mu)}, L_{\boldsymbol{\lambda}}^{(\mu)}, L_{\eta}^{(\mu)}\right)^T$ is the gradient of the Lagrangian function $L^{(\mu)}$ with respect to $\boldsymbol{\psi} := (\mathbf{u},\boldsymbol{\alpha},\boldsymbol{\lambda},\eta)^T$. Denoting by $\mathbf{e} := (1,\ldots,1)^T$the vector of all ones, $D_1 := \text{diag}\ (\alpha_i - \alpha_{min}^{(i)})$, and $D_2 := \text{diag}\ (\alpha_{max}^{(i)} - \alpha_i)$, the

diagonal matrices, we have

$$
\begin{aligned}
L_{\mathbf{u}}^{(\mu)} &= \nabla_{\mathbf{u}} J + A(\boldsymbol{\alpha})^T \boldsymbol{\lambda} = \mathbf{0} \ , \\
L_{\boldsymbol{\alpha}}^{(\mu)} &= \nabla_{\boldsymbol{\alpha}} J + \partial_{\boldsymbol{\alpha}} (\boldsymbol{\lambda}^T A(\boldsymbol{\alpha}) \mathbf{u}) + \eta \nabla_{\boldsymbol{\alpha}} c(\boldsymbol{\alpha}) - \mu^{-1} D_1^{-1} \mathbf{e} + \mu^{-1} D_2^{-1} \mathbf{e} = \mathbf{0} \ , \\
L_{\boldsymbol{\lambda}}^{(\mu)} &= A(\boldsymbol{\alpha}) \mathbf{u} - \mathbf{f} = \mathbf{0} \ , \\
L_{\eta}^{(\mu)} &= c(\boldsymbol{\alpha}) - C = 0 \ .
\end{aligned}
$$

The central path $\boldsymbol{\psi}(\mu) := (\mathbf{u}(\mu), \boldsymbol{\alpha}(\mu), \boldsymbol{\lambda}(\mu), \eta(\mu))^T$ depends on the parameter μ and solves the nonlinear system (36). For the solution procedure we apply the adaptive path-following predictor-corrector method explained in detail in [8] (p.248). We refer to [2] for recent applications of this method.

Predictor step: The predictor step relies on tangent continuation along the trajectory of the Davidenko equation

$$
F_{\boldsymbol{\psi}}(\boldsymbol{\psi}(\mu), \mu)\, \boldsymbol{\psi}'(\mu) = -F_{\mu}(\boldsymbol{\psi}(\mu), \mu). \tag{37}
$$

For a given approximation $\tilde{\boldsymbol{\psi}}(\mu_k)$ at $\mu_k > 0$, compute $\tilde{\boldsymbol{\psi}}^{(0)}(\mu_{k+1})$, where $\mu_{k+1} = \mu_k + \Delta\mu_k^{(0)}$, according to

$$
F_{\boldsymbol{\psi}}(\tilde{\boldsymbol{\psi}}(\mu_k), \mu_k)\, \delta\boldsymbol{\psi}(\mu_k) = -F_{\mu}(\tilde{\boldsymbol{\psi}}(\mu_k), \mu_k), \tag{38}
$$

$$
\tilde{\boldsymbol{\psi}}^{(0)}(\mu_{k+1}) = \tilde{\boldsymbol{\psi}}(\mu_k) + \Delta\mu_k^{(0)}\, \delta\boldsymbol{\psi}(\mu_k). \tag{39}
$$

We use $\Delta\mu_0^{(0)} = \Delta\mu_0$ for some given initial step-size $\Delta\mu_0$, whereas for $k \geq 1$ the predicted step-size $\Delta\mu_k^{(0)}$ is chosen by

$$
\Delta\mu_k^{(0)} := \left(\frac{\|\Delta\boldsymbol{\psi}^{(0)}(\mu_k)\|}{\|\tilde{\boldsymbol{\psi}}(\mu_k) - \tilde{\boldsymbol{\psi}}^{(0)}(\mu_k)\|} \, \frac{\sqrt{2}-1}{2\Theta(\mu_k)} \right)^{1/2} \Delta\mu_{k-1}, \tag{40}
$$

where $\Delta\mu_{k-1}$ is the computed continuation step-size, $\Delta\boldsymbol{\psi}^{(0)}(\mu_k)$ is the first Newton correction (see below), and $\Theta(\mu_k) < 1$ is the contraction factor associated with a successful previous continuation step.

Corrector step: As a corrector, we use Newton's method applied to $F(\boldsymbol{\psi}(\mu_{k+1}), \mu_{k+1}) = 0$ with $\tilde{\boldsymbol{\psi}}^{(0)}(\mu_{k+1})$ from (39) as a start vector. In particular, for $l \geq 0$ and $j_l \geq 0$ we compute $\Delta\boldsymbol{\psi}^{(j_l)}(\mu_{k+1})$ according to

$$F_{\boldsymbol{\psi}}(\tilde{\boldsymbol{\psi}}^{(j_l)}(\mu_{k+1}),\mu_{k+1})\,\Delta\boldsymbol{\psi}^{(j_l)}(\mu_{k+1}) = -F(\tilde{\boldsymbol{\psi}}^{(j_l)}(\mu_{k+1}),\mu_{k+1}) \qquad (41)$$

and $\bar{\Delta\boldsymbol{\psi}}^{(j_l)}(\mu_{k+1})$ as the associated simplified Newton correction

$$F_{\boldsymbol{\psi}}(\tilde{\boldsymbol{\psi}}^{(j_l)}(\mu_{k+1}),\mu_{k+1})\,\bar{\Delta\boldsymbol{\psi}}^{(j_l)}(\mu_{k+1}) = -F(\tilde{\boldsymbol{\psi}}^{(j_l)}(\mu_{k+1}) + \Delta\boldsymbol{\psi}^{(j_l)}(\mu_{k+1}),\mu_{k+1}). \qquad (42)$$

For the convergence of the Newton method we use the function

$$\Theta^{(j_l)}(\mu_{k+1}) := \|\bar{\Delta\boldsymbol{\psi}}^{(j_l)}(\mu_{k+1})\| \,/\, \|\Delta\boldsymbol{\psi}^{(j_l)}(\mu_{k+1})\|. \qquad (43)$$

In case of successful convergence, we accept the current step-size and proceed with the next continuation step. However, if the monotonicity test

$$\Theta^{(j_l)}(\mu_{k+1}) < 1 \qquad (44)$$

fails for some $j_l \geq 0$, the continuation step has to be repeated with the reduced step-size

$$\Delta\mu_k^{(l+1)} := \left(\frac{\sqrt{2}-1}{g(\Theta^{(j_l)})}\right)^{1/2} \Delta\mu_k^{(l)}, \qquad g(\Theta) := \sqrt{\Theta+1}-1 \qquad (45)$$

until we either achieve convergence or for a prespecified lower bound $\Delta\mu_{\min}$ observe

$$\Delta\mu_k^{(l+1)} < \Delta\mu_{\min}.$$

In the latter case, we stop the algorithm and report convergence failure.

At each inner iteration $l = 1, 2, \ldots$ until convergence, we apply inexact Newton's method for the solution of problems (41) and (42). We introduce additional multipliers $\mathbf{z} \geq \mathbf{0}$ and $\mathbf{w} \geq \mathbf{0}$ with respect to our inequality constraints and instead of the complementarity conditions $D_1\mathbf{z} = 0$ and $D_2\mathbf{w} = 0$ we consider

$$D_1\mathbf{z} \;=\; \mu^{-1}\,\mathbf{e} \quad , \quad D_2\mathbf{w} \;=\; \mu^{-1}\,\mathbf{e}\;. \qquad (46)$$

The relations (46) are called approximate complementarity, since for $\mu \to \infty$ they converge to the complementarity conditions that hold true at optimality.

Denoting by $L_{\mathbf{z}}^{(\mu)} := D_1\mathbf{z} - \mu^{-1}\mathbf{e}$, $L_{\mathbf{w}}^{(\mu)} := D_2\mathbf{w} - \mu^{-1}\mathbf{e}$, $Z := diag(z_i)$, and $W := diag(w_i)$, the Newton method results in the following primal-dual system

$$\underbrace{\begin{pmatrix} 0 & L_{\mathbf{u}\boldsymbol{\alpha}}^{(\mu)} & L_{\mathbf{u}\boldsymbol{\lambda}}^{(\mu)} & 0 & 0 & 0 \\ L_{\boldsymbol{\alpha}\mathbf{u}}^{(\mu)} & L_{\boldsymbol{\alpha}\boldsymbol{\alpha}}^{(\mu)} & L_{\boldsymbol{\alpha}\boldsymbol{\lambda}}^{(\mu)} & L_{\boldsymbol{\alpha}\eta}^{(\mu)} & -I & I \\ L_{\boldsymbol{\lambda}\mathbf{u}}^{(\mu)} & L_{\boldsymbol{\lambda}\boldsymbol{\alpha}}^{(\mu)} & 0 & 0 & 0 & 0 \\ 0 & L_{\eta\boldsymbol{\alpha}}^{(\mu)} & 0 & 0 & 0 & 0 \\ 0 & Z & 0 & 0 & D_1 & 0 \\ 0 & -W & 0 & 0 & 0 & D_2 \end{pmatrix}}_{\textbf{primal-dual system}} \begin{pmatrix} \Delta\,\mathbf{u} \\ \Delta\,\boldsymbol{\alpha} \\ \Delta\,\boldsymbol{\lambda} \\ \Delta\,\eta \\ \Delta\,\mathbf{z} \\ \Delta\,\mathbf{w} \end{pmatrix} = - \begin{pmatrix} L_{\mathbf{u}}^{(\mu)} \\ L_{\boldsymbol{\alpha}}^{(\mu)} \\ L_{\boldsymbol{\lambda}}^{(\mu)} \\ L_{\eta}^{(\mu)} \\ L_{\mathbf{z}}^{(\mu)} \\ L_{\mathbf{w}}^{(\mu)} \end{pmatrix}. \tag{47}$$

Since W and Z are diagonal matrices, static condensation of the approximate complementarity can be easily performed. Rearranging the unknowns according to $\mathbf{x} := (\mathbf{u}, \boldsymbol{\lambda})$ and $\mathbf{y} := (\boldsymbol{\alpha}, \eta)$, the resulting condensed primal-dual Hessian system can be written as the linear system

$$\begin{pmatrix} K_{\mathbf{xx}} & K_{\mathbf{xy}} \\ K_{\mathbf{yx}} & K_{\mathbf{yy}} \end{pmatrix} \begin{pmatrix} \Delta\mathbf{x} \\ \Delta\mathbf{y} \end{pmatrix} = - \begin{pmatrix} \mathbf{f}_1 \\ \mathbf{f}_2 \end{pmatrix}, \tag{48}$$

where

$$\begin{aligned} K_{\mathbf{xx}} &:= \begin{pmatrix} 0 & L_{\mathbf{u}\boldsymbol{\lambda}}^{(\mu)} \\ L_{\boldsymbol{\lambda}\mathbf{u}}^{(\mu)} & 0 \end{pmatrix}, \qquad K_{\mathbf{xy}} := \begin{pmatrix} L_{\mathbf{u}\boldsymbol{\alpha}}^{(\mu)} & 0 \\ L_{\boldsymbol{\lambda}\boldsymbol{\alpha}}^{(\mu)} & 0 \end{pmatrix}, \\ K_{\mathbf{yx}} &:= \begin{pmatrix} L_{\boldsymbol{\alpha}\mathbf{u}}^{(\mu)} & L_{\boldsymbol{\alpha}\boldsymbol{\lambda}}^{(\mu)} \\ 0 & 0 \end{pmatrix}, \qquad K_{\mathbf{yy}} := \begin{pmatrix} \tilde{L}_{\boldsymbol{\alpha}\boldsymbol{\alpha}}^{(\mu)} & L_{\boldsymbol{\alpha}\eta}^{(\mu)} \\ L_{\eta\boldsymbol{\alpha}}^{(\mu)} & 0 \end{pmatrix}, \\ \mathbf{f}_1 &:= \left(L_{\mathbf{u}}^{(\mu)}, L_{\boldsymbol{\lambda}}^{(\mu)}\right)^T, \qquad \mathbf{f}_2 := \left(\tilde{L}_{\boldsymbol{\alpha}}^{(\mu)}, L_{\eta}^{(\mu)}\right)^T. \end{aligned}$$

Here,

$$\begin{aligned} \tilde{L}_{\boldsymbol{\alpha}\boldsymbol{\alpha}}^{(\mu)} &:= L_{\boldsymbol{\alpha}\boldsymbol{\alpha}}^{(\mu)} + D_1^{-1}Z + D_2^{-1}W \quad , \\ \tilde{L}_{\boldsymbol{\alpha}}^{(\mu)} &:= L_{\boldsymbol{\alpha}}^{(\mu)} + D_1^{-1}L_{\mathbf{z}}^{(\mu)} - D_2^{-1}L_{\mathbf{w}}^{(\mu)} \quad . \end{aligned}$$

Note that $L_{\mathbf{u}\boldsymbol{\lambda}}^{(\mu)} = L_{\boldsymbol{\lambda}\mathbf{u}}^{(\mu)} = A(\boldsymbol{\alpha})$ is the stiffness matrix and hence, the first diagonal block $K_{\mathbf{xx}}$ is indefinite, but nonsingular. The resulting primal-dual linear system (48) is solved by a null-space approach using right transforming iterations (originally proposed in [17]) with respect to the special block

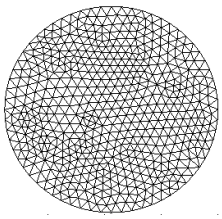

Figure 5. Unstructured grid generated in the domain Ω

structure of the primal-dual Hessian. Applications of this method together with a line-search approach after computation of the Newton increments are described in detail in [12, 13].

5 Numerical experiments

In this section, we consider the problem to compute the optimal distribution of our composite material in a given domain. Let $\Omega \subset \mathcal{R}^2$ be a suitable chosen domain that allows to introduce surface traction $\mathbf{t}$ applied to $\Gamma_T \subset \partial\Omega$, as shown on Figure 4. On the remaining portion Γ_D of the boundary the displacements $\mathbf{g}$ are specified.

In our numerical experiments, the domain Ω is chosen to be a circle which corresponds naturally to a cross section of our original wood structure, see Figure 5. Unstructured triangular grid is generated in the domain. We impose homogeneous boundary conditions on the Dirichlet nodes and inhomogeneous Neumann boundary conditions on the loading surface.

We consider the mean compliance of the structure defined as follows

$$J(\mathbf{u}, \boldsymbol{\alpha}) = \int_\Omega \mathbf{f} \cdot \mathbf{u}\, dx + \int_{\Gamma_T} \mathbf{t} \cdot \mathbf{u}\, ds, \tag{49}$$

where $\mathbf{f}$ is the external body force applied to Ω. The displacement vector $\mathbf{u} = (u_1, u_2)^T$ represents the state variables, and the vector $\boldsymbol{\alpha} = (\alpha_1, \alpha_2)^T$ stands for the design parameters α_1 and α_2, the widths of the carbon- and SiC-layers, respectively, see Figure 3.

The microcell Y is fixed as the unit square, i.e. $Y = [0, 1] \times [0, 1]$. We stated at the end of Section 2 that the computation of $\boldsymbol{\xi} = (\xi_p^{k\ell})_{k,\ell,p=1}^2$ as the solution of (20) has to de done numerically. For this purpose, we discretize the periodicity cell problems (20) by continuous, piecewise linear finite elements with respect to an adaptively generated simplicial triangulation $\mathcal{T}_h$ of Y. Note that adaptive grid refinement pays off due to the occurrence of both reentrant corners and jumps in the elasticity coefficients across interior interfaces (ma-

Table 2. Convergence results: $\alpha_1^{(0)} = \alpha_2^{(0)} = 0.1,\ C = 0.3$

k	α_1	α_2	$\|L_{\boldsymbol{\lambda}}^{(\mu)}\|$	$\|L_{\eta}^{(\mu)}\|$	$\|L_{\mathbf{z}}^{(\mu)}\|$	$\|L_{\mathbf{w}}^{(\mu)}\|$	μ^{-1}	J	$\|\mathbf{F}^{(\mu)}\|$
1	0.212	0.08	4.915	1.0e-3	0.831	1.141	0.144	27.47	145.2
2	0.059	0.24	20.20	1.1e-5	0.053	0.757	0.061	3.79	38.53
3	5.8e-4	0.29	4.032	8.2e-6	0.026	0.478	0.027	2.73	23.47
4	5.9e-6	0.29	2.260	4.7e-6	0.023	0.038	4.4e-3	1.94	8.57
5	9.3e-5	0.29	0.012	9.5e-9	5.1e-3	5.1e-3	9.1e-4	1.25	0.06
6	1.8e-5	0.29	2.6e-5	7.e-13	1.0e-3	1.0e-3	1.8e-4	1.25	0.05
7	3.6e-6	0.29	1.1e-5	5.e-14	2.3e-4	2.3e-4	1.3e-5	1.25	0.01
8	2.6e-7	0.29	5.6e-8	5.e-17	1.8e-5	1.8e-5	7.1e-8	1.24	2.0e-3
9	1.4e-9	0.29	3.4e-10	0.0	1.e-7	1.1e-7	2.e-12	1.24	1.9e-4
10	5.e-14	0.3	1.4e-13	0.0	3.e-12	4.e-12	3.e-21	1.24	1.0e-6

terial interfaces). Here, the grid refinement is based on the Zienkiewicz-Zhu (ZZ) a posteriori error estimator (cf. [19]). The adaptive refinement process is visualized on Figure 6.

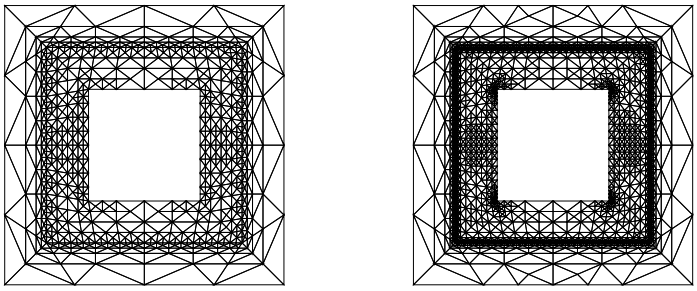

Figure 6. Adaptive refinement triangulation in Y, density 84%, a) 7 adaptive levels, 1346 triangles, 697 nodes; b) 10 adaptive levels, 2888 triangles, 1480 nodes

In Table 2 we present some convergence results for initial values of the widths of the carbon and silicon carbide layers $\alpha_1 = \alpha_2 = 0.1$ and a constant $C = 0.3$ in (27). We report the number of outer iterations k in the continuation method, the computed values of the widths of the layers α_1 and α_2, the l_2-norm of the gradient of the Lagrangian with respect to the Lagrangian multipliers and the complementarity variables, the value of the barrier parameter, the final value of the objective functional J, and the l_2-norm of the global gradient of L. We notice that the computed value α_1 of the carbon layer goes to zero, i.e. the solid part of the body is entirely occupied by the silicon carbide layer which is natural due to the higher stiffness of this material.

Similar computational results can be observed in Table 3 where we vary the values of the initial widths $\alpha_1^{(0)}$ and $\alpha_2^{(0)}$ of the material layers and the constant C in the equality constraint (27). We present in this table the final number of outer iterations k, the computed widths of the carbon- and SiC-layers (respectively, α_1 and α_2), the final value of the barrier parameter μ^{-1},

Table 3. Convergence results for biomorphic microcellular SiC ceramics

$\alpha_1^{(0)}$	$\alpha_2^{(0)}$	C	k	α_1	α_2	μ^{-1}	J	$\|\mathbf{F}^{(\mu)}\|$	$\|\mathbf{v}\|$
0.07	0.07	0.4	13	1.1e-11	0.4	6.3e-17	0.85	1.52e-5	e-10
0.15	0.15	0.2	12	8.7e-17	0.2	3.4e-23	2.34	1.24e-8	e-9
0.15	0.25	0.3	11	4.4e-13	0.3	2.1e-19	1.24	3.26e-6	e-6
0.25	0.05	0.4	19	1.7e-13	0.4	1.0e-21	0.85	3.16e-4	e-4
0.30	0.05	0.1	15	3.7e-17	0.1	1.0e-25	7.73	1.55e-8	e-8
0.20	0.15	0.4	11	1.7e-13	0.4	1.3e-20	0.85	1.69e-6	e-6
0.40	0.01	0.2	15	2.6e-12	0.2	3.2e-17	2.34	1.15e-5	e-6

the value of the objective functional J at the last continuation step, the l_2-norms of the gradient $\mathbf{F}^{(\mu)}$ of the Lagrangian function and the complementarity multipliers $\mathbf{v} = (\mathbf{z}, \mathbf{w})$. In the numerical experiments we initialize the barrier parameter by $\mu_0 = 1$.

6 Conclusions

We have considered a shape optimization of biomorphic ceramic composites. Our materials are produced using a naturally grown wood by a two-steps processing: high-temperature pyrolysis of the wooden specimen and infiltration reaction of the carbonized wood with a carbide forming metal, for instance, silicon. Our purpose was to find the optimal material-and-shape distribution in a given domain which is occupied by periodically distributed constituents.

The macroscopic homogenized model is obtained by the homogenization approach assuming an asymptotic expansion of the solution of the nonhomogenized elasticity equation with a scale parameter close to zero. The lengths and widths of the different material layers forming the cell walls are considered as design parameters. These variables can be tuned very precisely during the processing and have a significant impact on the macroscopic mechanical behavior of the final ceramics. The homogenized elasticity equation is considered as an equality constraint in the shape optimization problem. Additionally, we have inequality constraints motivated by the microstructural geometry.

Interior-point methods have been chosen for the solution of the PDE constrained optimization problem. We focus on barrier methods that are used to transform constrained problems to unconstrained ones. They typically give rise to parameterized families of approximate subproblems whose solutions converge asymptotically to the exact solution along centered paths. For the parameter-dependent nonlinear system we apply a path-following predictor-corrector strategy. For the prediction step we rely on a tangent continuation along the trajectory of the solution of the Davidenko equation. If the predicted step-size is too large, a correction is performed by using the Newton method within an appropriate monotonicity test.

Acknowledgments

This work has been partially supported by the German National Science Foundation (DFG) under Grant HO877/5-3. The research of the second author has been sponsored in part by Grant I1402/2004 of the Bulgarian Ministry for Education and Science.

References

[1] Allaire, G., 2002, *Shape Optimization by the Homogenization Method*, Springer, Berlin-Heidelberg-New York.
[2] Antil, H., Hoppe, R.H.W. and Linsenmann, Chr., 2007 *Path-following primal-dual interior-point methods for shape optimization*, J. Numer. Math. **15** (to appear).
[3] Bakhvalov, N. and Panasenko, G., 1984, *Averaging Processes in Periodic Media*, Nauka, Moscow.
[4] Bendsøe, M.P., 1995. *Optimization of Structural Topology, Shape, and Material*, Springer, Berlin.
[5] Bensoussan, A., Lions, J.L. and Papanicolaou, G., 1978, *Asymptotic Analysis for Periodic Structures*, Elsevier Science Publishers, North-Holland, Amsterdam.
[6] Byrd R.H., Hribar, M.E. and Nocedal, J., 1999, *An interior point algorithm for large scale nonlinear programming*, SIAM J. Optim., **9**(4), 877-900.
[7] Delfour, M.C. and Zolesio, J.P., 2001, *Shapes and Geometries: Analysis, Differential Calculus, and Optimization*, SIAM, Philadelphia.
[8] Deuflhard, P., 2004, *Newton Methods for Nonlinear Problems. Affine Invariance and Adaptive Algorithms*, Springer, Berlin-Heidelberg-New York.
[9] El-Bakry, A., Tapia, R., Tsuchiya, T. and Zhang Y., 1996, *On the formulation and theory of the Newton interior-point method for nonlinear programming*, J. Optim. Theory Appl., **89**, 507-541.
[10] Forsgren, A., Gill, P.E. and Wright, M.H., 2002, *Interior methods for nonlinear optimization*, SIAM Review, **44**, 525-597.
[11] Jikov, V.V., Kozlov, S.M. and Oleinik, O.A., 1994, *Homogenization of Differential Operators and Integral Functionals*, Springer.
[12] Hoppe, R.H.W. and Petrova, S.I., 2004, *Optimal shape design in biomimetics based on homogenization and adaptivity*, Math. Comput. Simul., **65**, 257-272.
[13] Hoppe, R.H.W. and Petrova, S.I., 2004, *Primal-dual Newton interior point methods in shape and topology optimization*, Numer. Linear Algebra Appl., **11**(5-6), 413-429.
[14] Mohammadi, B. and Pironneau, O., 2001, *Applied Shape Optimization for Fluids*, Oxford University Press, Oxford.
[15] Pankov, A., 1997, *G-convergence and Homogenization of Nonlinear Partial Differential Operators*, Kluwer, Dordrecht.
[16] Sokolowski, J. and Zolésio, J.-P., 1992, *Introduction to Shape Optimization*, Springer Series in Computational Mathematics, Vol. 16, Springer.
[17] Wittum, G., 1989, *On the convergence of multigrid methods with transforming smoothers. Theory with applications to the Navier-Stokes equations*, Numer. Math., **57**, 15-38.
[18] Wright, M.H., 1992, *Interior methods for constrained optimization*, Acta Numerica, **1**, 341-407.
[19] Zienkiewicz, O.C. and Zhu, J.Z., 1987, *A simple error estimator and adaptive procedure for practical engineering analysis*, Intern. J. Numer. Methods Eng., **24**, 337-357.